

RESEARCH ARTICLE

10.1002/2016JA022980

Key Points:

- Detection of electron-depleted dusty ion-ion plasma in lower ionosphere with enhanced densities
- First empirical estimate of the negative ion and dust grain charge

Correspondence to:

O. Shebanits,
oleg.shebanits@irfu.se

Citation:

Shebanits, O., et al. (2016), Ion and aerosol precursor densities in Titan's ionosphere: A multi-instrument case study, *J. Geophys. Res. Space Physics*, 121, 10,075–10,090, doi:10.1002/2016JA022980.

Received 20 MAY 2016

Accepted 3 SEP 2016

Accepted article online 10 SEP 2016

Published online 8 OCT 2016

Ion and aerosol precursor densities in Titan's ionosphere: A multi-instrument case study

O. Shebanits^{1,2}, J.-E. Wahlund¹, N. J. T. Edberg¹, F. J. Crary³, A. Wellbrock^{4,5}, D. J. Andrews¹, E. Vigren¹, R. T. Desai^{4,5}, A. J. Coates^{4,5}, K. E. Mandt^{6,7}, and J. H. Waite Jr⁶

¹Swedish Institute of Space Physics, Uppsala, Sweden, ²Department of Physics and Astronomy, Uppsala University, Uppsala, Sweden, ³University of Colorado Boulder, Boulder, Colorado, USA, ⁴Mullard Space Science Laboratory, University College London, London, UK, ⁵Centre for Planetary Sciences, University College London/Birkbeck, London, UK, ⁶Space Science and Engineering Division, Southwest Research Institute, San Antonio, Texas, USA, ⁷Department of Physics and Astronomy, University of Texas at San Antonio, San Antonio, Texas, USA

Abstract The importance of the heavy ions and dust grains for the chemistry and aerosol formation in Titan's ionosphere has been well established in the recent years of the Cassini mission. In this study we combine independent in situ plasma (Radio Plasma and Wave Science Langmuir Probe (RPWS/LP)) and particle (Cassini Plasma Science Electron Spectrometer, Cassini Plasma Science Ion Beam Spectrometer, and Ion and Neutral Mass Spectrometer) measurements of Titan's ionosphere for selected flybys (T16, T29, T40, and T56) to produce altitude profiles of mean ion masses including heavy ions and develop a Titan-specific method for detailed analysis of the RPWS/LP measurements (applicable to all flybys) to further constrain ion charge densities and produce the first empirical estimate of the average charge of negative ions and/or dust grains. Our results reveal the presence of an ion-ion (dusty) plasma below ~1100 km altitude, with charge densities exceeding the primary ionization peak densities by a factor ≥ 2 in the terminator and nightside ionosphere ($n_e/n_i \leq 0.1$). We suggest that ion-ion (dusty) plasma may also be present in the dayside ionosphere below 900 km ($n_e/n_i < 0.5$ at 1000 km altitude). The average charge of the dust grains (≥ 1000 amu) is estimated to be between -2.5 and -1.5 elementary charges, increasing toward lower altitudes.

1. Introduction

Titan, the largest moon of Saturn, has attracted considerable scientific attention over the duration of the Cassini mission. Titan hosts a fully developed dense atmosphere [Niemann *et al.*, 2005], and a substantial ionosphere was detected already by the Voyager 1 spacecraft [Bird *et al.*, 1997]. The ionosphere extends up to approximately 2200 km altitude [Wahlund, 2005; Edberg *et al.*, 2010; Galand *et al.*, 2014, and references therein], almost a full radius of the moon, and is produced mainly by the solar EUV on the dayside [Cravens, 2005; Ågren *et al.*, 2009; Shebanits *et al.*, 2013; Vigren *et al.*, 2015] and energetic particle impacts on the nightside [Ågren *et al.*, 2007; Cravens *et al.*, 2009], although Saturn's magnetospheric dynamics and the Saturn local time of Titan are also important [Edberg *et al.*, 2015]. The energy inputs initiate a complex organic chemistry [Cravens *et al.*, 2006, 2009; Cui *et al.*, 2009; Magee *et al.*, 2009; Vuitton *et al.*, 2009; Mandt *et al.*, 2012], which contributes to the synthesis of aerosols in Titan's orange haze at altitudes of ~500 km [e.g., Niemann *et al.*, 2005; Coates *et al.*, 2009; Lavvas *et al.*, 2013]; in particular, heavy ions and dust grains play key roles in the aerosol formation in Titan's ionosphere [e.g., Coates *et al.*, 2007; Waite *et al.*, 2007; Sittler *et al.*, 2009; Wahlund *et al.*, 2009; Gudipati *et al.*, 2013; Lavvas *et al.*, 2013; Wellbrock *et al.*, 2013].

Using the Cassini Plasma Science Electron Spectrometer (CAPS/ELS) mass/charge spectra, the negative charge carriers can be grouped into negative ions (distinct spectral peaks) with masses < 100 amu and the heavy negative ions (continuous spectra) with masses > 100 amu; the latter have been identified as nanometer-sized dust aerosol precursors [Lavvas *et al.*, 2013]. The positive ions can be grouped in a similar way based on the Cassini Plasma Science Ion Beam Spectrometer (CAPS/IBS) mass/charge spectra, with masses > 100 amu also contributing to the aerosol growth [Wahlund *et al.*, 2009; Lavvas *et al.*, 2013]. The lower region of Titan's ionosphere at < 1200 km (altitude) is known to be populated by heavy (up to 13,800 amu/charge) negative ions [Coates *et al.*, 2007, 2009, 2010; Wellbrock *et al.*, 2013] and a dusty ion-ion plasma [Ågren *et al.*, 2012; Shebanits *et al.*, 2013]. We define the plasma dusty when the dust grain radius is much smaller than the intergrain distance, which is in turn smaller than the dust Debye length [Shukla and Mamun, 2002].

The altitude and solar zenith angle (SZA) dependencies of the heavy negative charge carrier densities in Titan's ionosphere have been analyzed by *Shebanits et al.* [2013] and *Wellbrock et al.* [2013]. However, the charge of the heavy negative ions and dust grains cannot be uniquely identified by the CAPS/ELS as it measures energy/charge and has so far only been inferred theoretically. Based on the CAPS/ELS mass spectra from T16 to T19 and assuming grain potential based on the Radio Plasma and Wave Science Langmuir Probe (RPWS/LP) electron temperature measurements during the TA flyby ($T_e \sim 1000$ K) the negative ion charge was estimated to ~ 1 – 5 elementary charges [Coates et al., 2007]; similar estimate of the grain potential was carried out based on the Ion and Neutral Mass Spectrometer (INMS) mass spectra from T16 to T23 and assuming an electron temperature of 125 K [Waite et al., 2007]. However, direct measurements of the electron temperatures by the RPWS/LP show typical values in Titan's ionosphere in the range of 300–600 K below 1100 km based on 52 flybys [Edberg et al., 2010], with instrumental uncertainty of the lowest temperatures at ~ 170 K or 0.015 eV [Galand et al., 2014], and at altitudes below 1000 km the theoretical calculations suggest the electron, ion, and neutral temperatures to be ≈ 150 K [Richard et al., 2011]; a lower T_e would lower the estimated grain potential (and therefore the charge) proportionally. Using direct measurements of the spacecraft (S/C) potential by the RPWS/LP (typical values between -1 V and -0.5 V [see e.g., Ågren et al., 2007, 2012; Wahlund et al., 2009; Edberg et al., 2011]) as a proxy for the dust grain potential based on 47 flybys below 1100 km, the negative dust grain charge was estimated to 1–2 elementary charges [Shebanits et al., 2013] from a general case of a dusty plasma in electrostatic equilibrium [Whipple et al., 1985; Horányi et al., 2004]. The average mass of ions (in the RPWS/LP data analysis) has previously been derived from INMS data [Shebanits et al., 2013], which gives a good flyby coverage but is limited to lighter positive ions (< 99 amu) [Mandt et al., 2012], resulting in a lower limit of the charge densities of positive and negative ions. Heavier negative ions can be included by using the CAPS/ELS and positive ions by using CAPS/IBS data, but the CAPS instrument was turned off in June 2012, greatly limiting the flyby coverage.

In this study we present a method for detailed analysis of the RPWS/LP ion data from Titan's ionosphere. The method addresses the issues described above and gives constrained values of the positive and negative ion (aerosol precursor) charge densities, mean ion mass profiles, and the first empirical charge estimate of the negatively charged species. We apply this method to four flybys where data from RPWS/LP, CAPS/ELS, and CAPS/IBS are simultaneously available: T16, T29, T40, and T56, chosen as representatives of dayside (T40), terminator (T16), and nightside regions (T29 and T56). The involved instruments are briefly described in section 2; the method is described in section 3, with supporting information in the Appendix. The results are presented and discussed in section 4, and summarized in section 5.

2. Instruments

The method presented here was developed by using data sets from INMS and simultaneous in situ measurements by CAPS/IBS, CAPS/ELS, and RPWS/LP. The ion mass profiles of positive ions were provided by the INMS (up to 99 amu) and CAPS/IBS, and of negative ions by the CAPS/ELS; CAPS/ELS also provided the profiles of densities per charge of negative ions. The RPWS/LP provided the charge densities of both positive and negative ions.

2.1. Radio Plasma and Wave Science Langmuir Probe (RPWS/LP)

Part of the RPWS package on board the Cassini S/C, the RPWS/LP is a spherical probe with diameter of 2.5 cm, mounted on a 1.5 m boom [Gurnett et al., 2004; Wahlund et al., 2009; Morooka et al., 2011]. The probe measures the current of charged particles in two modes: voltage sweeps and 20 Hz current sampling at a fixed bias voltage. The 20 Hz current sampling is performed between the voltage sweeps and usually measures electron current at a set bias potential of +11.5 V. The voltage sweep samples the total incoming/outgoing current from plasma as a function of applied bias voltage (photoelectron current removed in the analysis): ± 32 V in 512 steps under 0.5 s every 10 min in Saturn's magnetosphere and ± 4 V every 24 s during targeted flybys, shifting the voltage from +4 V to -4 V and back to +4 V (double sweeps) in 1024 steps under 1 s. For Titan flybys this gives the spatial resolution of ≈ 3 km (due to the S/C velocity ≈ 6 km/s). The current-voltage characteristic inferred from the positive voltage part of the sweeps gives electron density and temperature as well as a proxy for the S/C potential; from the negative voltage part the ion charge densities are derived, both positively charged ions and negatively charged ions/particles (ion ram energy is ≥ 5 eV).

In this study we have used the ion charge densities and the S/C potential from the voltage sweep operation mode for the selected flybys (T16, T29, T40, and T56).

2.2. Ion and Neutral Mass Spectrometer (INMS)

INMS is a high-resolution quadrupole mass analyzer, a particle instrument for measuring mass spectra of neutral gas and positive ions in the range of 1–99 amu. The mean positive ion mass data are provided from measurements in the open ion source mode, where the ions are focused into the quadrupole mass analyzer by the quadrupole switching lens and separated by the mass-to-charge ratios [Waite *et al.*, 2004; Mandt *et al.*, 2012]. The mean positive ion mass profiles are derived by using INMS measurements from 14 flybys (T5, T17, T18, T21, T26, T32, T36, T39, T40, T48, T50, T51, T57, and T59). These are consequently used to produce the mean mass profiles for the selected flybys (T16, T29, T40, and T56) through an exponential altitude-SZA fit [Shebanits *et al.*, 2013].

2.3. Cassini Plasma Science Electron Spectrometer (CAPS/ELS)

Part of the CAPS package, the ELS is a hemispherical top-hat electrostatic analyzer. During a measurement, ELS sweeps through quasi-logarithmically spaced voltages (63 energy bins) in accumulation intervals of 31.25 ms (25% “dead time” to allow the sweep high voltage to settle and 75% active accumulation); for Titan, the default mode is 0.6 eV/q–28 keV/q in 64 steps [Linder *et al.*, 1998; Young *et al.*, 2004; Coates *et al.*, 2007], giving a spatial resolution of ~ 8 km (due to the S/C velocity). The duration of the negative signatures observed by the CAPS/ELS varies but is typically 16 s. This results in an altitude uncertainty of ± 20 km, ± 10 km for most cases [Wellbrock *et al.*, 2013]. The $\Delta E/E$ energy resolution is 17%, which translates into the same value for the $\Delta m_-/m_-$ mass resolution of the negative charge carriers [Linder *et al.*, 1998; Young *et al.*, 2004]. ELS detects energy/charge of negative charge carriers. In the case of the negative ions and dust grains, the observed energy/charge can be converted to mass/charge and the recorded counts (electron background subtracted) to density/charge by interpreting the counts as a current [Coates *et al.*, 2007; Wellbrock *et al.*, 2013]. This conversion is different to the way electron densities are calculated from counts via integrating the particle distribution function [Lewis *et al.*, 2008]. The charge dependency of the CAPS/ELS measurements is of particular importance as the heavier species may have multiple charges. ELS was designed to measure electrons, and therefore, the microchannel plate (MCP) efficiency for negative ions and dust grains is not well understood, leading to uncertainties on the densities with the currently estimated values providing a likely upper limit. The dominant uncertainty on the negative ion mass is the energy bin size, i.e., 17%. In this study we use the conservative density uncertainty estimate of 50% [Wellbrock *et al.*, 2013].

2.4. Cassini Plasma Science Ion Beam Spectrometer (CAPS/IBS)

Similarly to CAPS/ELS, the IBS is a curved-electrode electrostatic analyzer, designed for high-resolution measurements of positive ion flux over 0.6 eV/q–28 keV/q energy range, from which mass/charge and density/charge profiles are derived. During operation the instrument performs a voltage scan in 255 steps over 2 s [Young *et al.*, 2004], giving a spatial resolution at Titan ~ 12 km (due to the S/C velocity). The $\Delta E/E$ energy resolution is 1.4%, which translates into the same value for the $\Delta m_+/m_+$ mass resolution [Young *et al.*, 2004]. The 10–20% uncertainties in density/charge may arise due to ion drifts perpendicular to Cassini trajectory, the effect of these would be scaling of the spectra (due to changed particle energy) but the relative abundance is unaffected (i.e., drifts do not shift the mass peaks), and mass/charge is cross-calibrated with INMS [Crary *et al.*, 2009]. In Titan’s ionosphere, the energy of ions is up to 207 eV/q (primarily ram energy), which translates to ≈ 1100 amu [Crary *et al.*, 2009], assuming stationary singly charged positive ions [Thissen *et al.*, 2011].

3. Method

The primary goals of the method presented here are as follows:

1. to improve the analysis of RPWS/LP current-voltage characteristics for negative probe bias (ion current) using the ion mass measurements from the particle instruments (INMS, CAPS/IBS, and CAPS/ELS), for applications in Titan’s ionosphere and similar plasma conditions (described in section 3.1);
2. to construct altitude profiles of mean ion mass for positive and negative ions, with heavy ions included, that is applicable to all Titan flybys (section 3.2);

3. to infer the mean charge of the negative charge carriers: negative ions and nanometer-size dust grains (aerosol precursors) (section 3.4).

3.1. Ion Current Response of the RPWS/LP

Using the positive and negative mass/q distributions from CAPS/IBS and CAPS/ELS, respectively, it is possible to model the ion currents to RPWS/LP. According to the orbital motion limited (OML) theory for a spherical probe [Mott-Smith and Langmuir, 1926; Medicus, 1962], the total ion current is derived by integrating the Maxwellian velocity distribution of the plasma particles reaching the probe [see, e.g., Whipple, 1965; Engwall, 2006]. Here we adapt the equation (3.26) from Engwall [2006] (see Appendix for details):

$$I = -qn r_{ip}^2 \sqrt{\frac{\pi k_B T}{2m}} \left[e^{-A^2} \left(1 - \frac{v_1}{v_{sc}} \right) + e^{-B^2} \left(1 + \frac{v_1}{v_{sc}} \right) + \sqrt{\frac{\pi k_B T}{2m v_{sc}^2}} \left(\frac{m v_{sc}^2}{k_B T} + 1 - \frac{2qU}{k_B T} \right) (\text{erf}(A) - \text{erf}(B)) \right], \quad (1)$$

where I is the collected current of an ion species for a probe potential U ; q , n , m , v , and T are ion charge, density, mass, speed, and temperature, respectively; r_{ip} is the probe radius; k_B is the Boltzmann constant; v_{sc} is the spacecraft speed relative to the plasma, $A = \sqrt{\frac{m}{2k_B T}}(v_1 + v_{sc})$; $B = \sqrt{\frac{m}{2k_B T}}(v_1 - v_{sc})$; $\text{erf}(x) = \frac{2}{\sqrt{\pi}} \int_0^x e^{-y^2} dy$; and v_1 is the minimum relative speed a particle needs to overcome the potential barrier defined as $v_1 = \sqrt{2qU/m}$ for repelling potentials and zero otherwise. The total ion current is obtained by summing over all ions (by mass). Equation (1) is not used in the RPWS/LP ion analysis; however, the measured ion current depends linearly on the bias voltage of RPWS/LP (except T70 that showed a slight deviation, possibly due to a differential drift of positive and negative charge carriers [see Ågren *et al.*, 2012]), and it is sufficient to use a numerically convenient approximation of the ion current [Fahleson *et al.*, 1974] for the RPWS/LP ion analysis (see also Appendix in Shebanits *et al.* [2013]):

$$I = -qn\pi r_{ip}^2 |v_{sc}| \left(1 - \frac{2q|U|}{m v_{sc}^2} \right) \quad (2)$$

This approximation is specific to the dense cold plasma of Titan's ionosphere, under the following assumptions:

1. The negative ion current is approximated as linear because the ion current measured by the RPWS/LP does not express exponential trend for the negative bias potential down to -4 V (typical Titan operation) with an exception of T70 [Ågren *et al.*, 2012].
2. The thermal ion current to the RPWS/LP is negligible compared to the ram ion current in Titan's ionosphere as the thermal energies of ions are <0.1 eV [Crary *et al.*, 2009; Edberg *et al.*, 2010; Galand *et al.*, 2014, and references therein], while the ram energies are >5 eV.
3. Ions and neutrals are assumed to be stationary in Titan's ionosphere (typical neutral winds and ion drifts below 1400 km altitudes are ~ 260 ms^{-1} [Müller-Wodarg *et al.*, 2006, 2008; Crary *et al.*, 2009] compared to the S/C speed of ≈ 6 km s^{-1}).

The ion current modeled with equation (1) is used to test the limits of the approximation (equation (2)). OML is applicable for RPWS/LP for electron Debye lengths (λ_{De}) larger than the probe radius ($r_{ip} = 2.5$ cm for RPWS/LP), which is indeed the case for Titan's ionosphere ($\lambda_{De} \geq 3$ cm) [Shebanits *et al.*, 2013]. For λ_{De} much smaller than the probe radius the plasma sheath around the probe sets up potential barriers that changes the collected currents and the Sheath Limited theory must be used instead [Laframboise and Parker, 1973]. However, since the ion currents are dominated by the ram flux to the probe, this applies mainly to the electron currents.

3.2. Ion Mass Considerations

The RPWS/LP offers a large coverage of Titan flybys and an in situ data set of ionospheric plasma parameters. To infer accurate positive and negative ion charge densities from the RPWS/LP characteristic, the respective ion mass distributions are required due to nonlinear mass dependence of the sampled ion current. To that end it is possible to use the CAPS/IBS-derived positive ion mass (Figure 1) and the negative ion mass from CAPS/ELS (Figure 2). However, the CAPS instrument was turned off in June 2012. To address the issue we have selected four flybys where in situ measurements by INMS [Shebanits *et al.*, 2013, Figure 3], CAPS/ELS, CAPS/IBS, and RPWS/LP, were available. The chosen flybys represent Titan's ionosphere at dayside (T40,

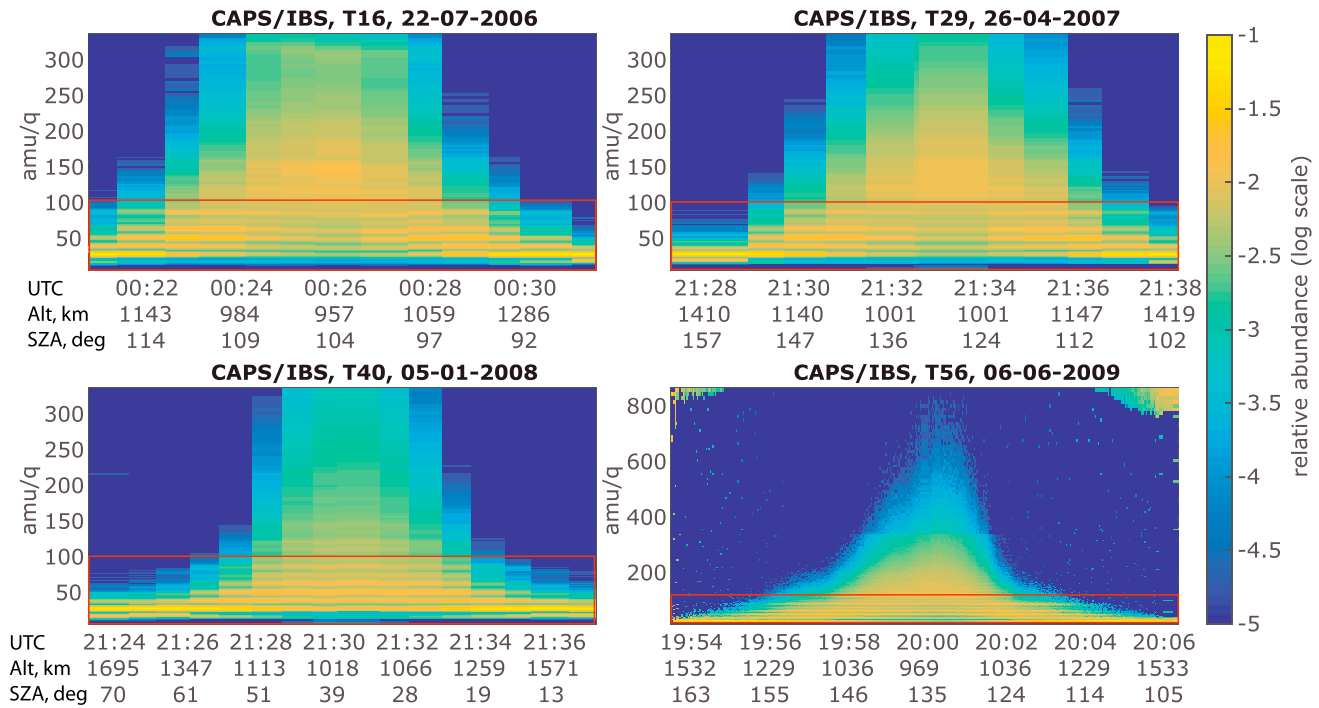


Figure 1. CAPS/IBS positive ion abundance by mass for flybys T16, T29, T40, and T56. The red outline represents the mass range of INMS.

SZA < 70°), terminator (T16, 90°–120° SZA), and nightside (T29 and T56, SZA > 100°). Since the heavier ions are produced from the lighter ions, a dependency is expected between the mean ion masses derived from the INMS measurements and those derived from the CAPS measurements. Combining the CAPS and INMS data for the four selected flybys we indeed find such a dependency (Figures 3a and 3b), an exponential trend inversely proportional to altitude. The altitude trend in Figure 3b is in agreement with that reported by the CAPS/ELS team [Wellbrock et al., 2013]. Applying these trends to the the INMS-derived mean ion mass altitude profiles includes the heavy ions/charge carriers and produces equivalents of the profiles derived with CAPS/IBS and CAPS/ELS, applicable to all flybys (Figures 3c and 3d). However, using the mean ion mass to derive the total ion densities in the models results in a mismatch of the ion current slope between the model and the measurements. The mean ion mass profiles are therefore insufficient at altitudes below 1200 km even after the inclusion of the heavier ions. For the purposes of RPWS/LP ion analysis the required ion mass

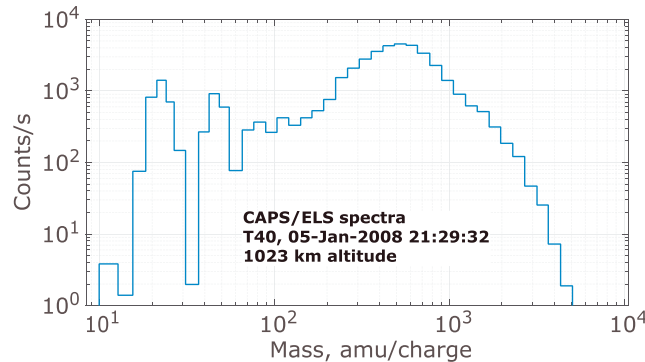


Figure 2. CAPS/ELS spectrum of a T40 low-altitude (1023 km) negative ion signature at 21:29:32 UTC. The ELS energy (i.e., mass) bins are spaced logarithmically; hence, the higher mass bins contain a larger range of masses than the lower mass bins. The continuous spectra of negative ions with masses >100 amu/q identifies them as nanometer-sized dust particles [Lavvas et al., 2013].

is actually not the mean ion mass but effective ion mass because summing the ion currents means that the masses are added as Σm^{-1} (see derivation below). The effective ion mass cannot be related to the mean ion mass mathematically, and it is impossible to calculate the effective ion mass exactly without the CAPS mass distribution spectra for each measurement point. It is possible, however, to derive the effective ion mass empirically as a function of the INMS mean ion mass, which can then be used for any flyby. These are plotted versus altitude in Figures 3c and 3d. It should be noted that due to differential S/C charging an additional corrective factor may be required for

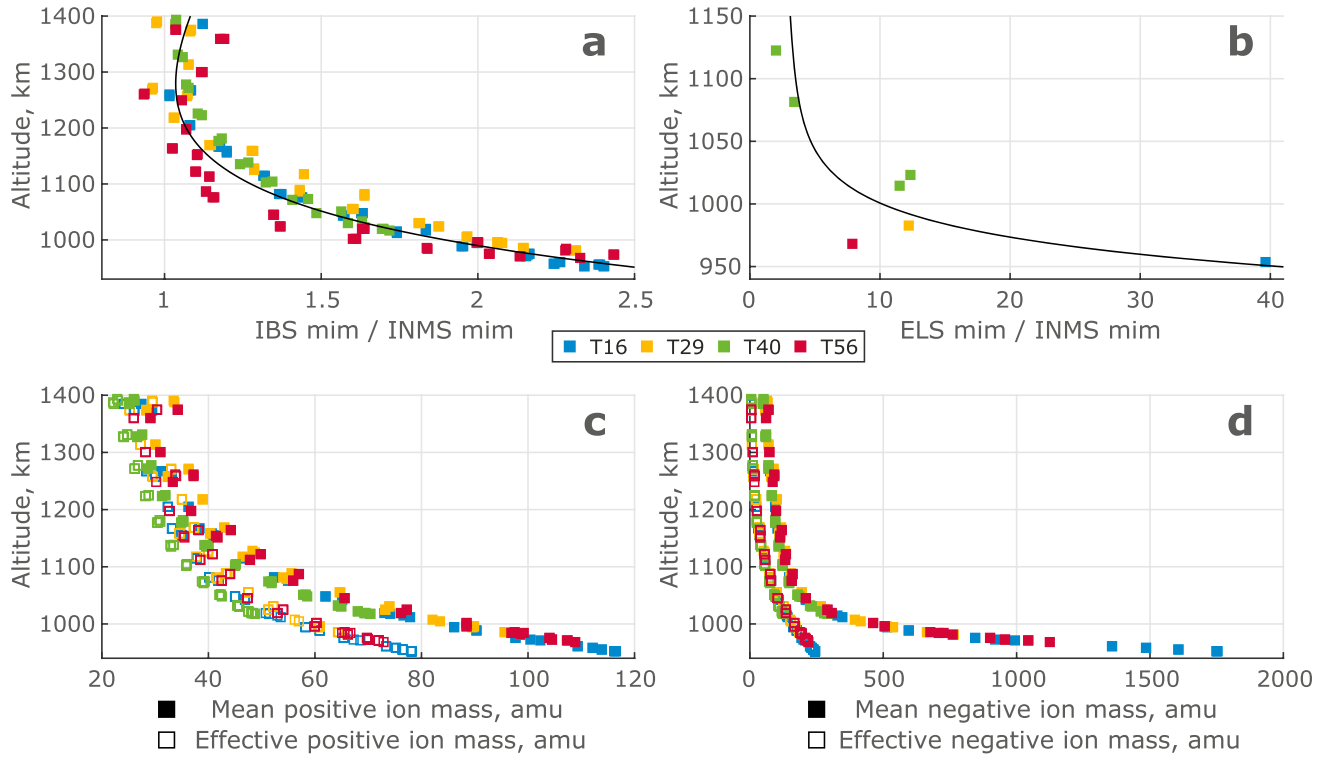


Figure 3. Mean ion mass ratios as functions of altitude: IBS to INMS, (a) positive ions and ELS to INMS, (b) negative ions/charge carriers, and mean ion masses derived from them: (c) positive and (d) negative mean (filled squares) and effective mass (empty squares) altitude profiles of the respective charge carriers. All flybys profiles are color-coded according to the legend. The mass profiles in Figures 3c and 3d are derived from the fits to the profiles in Figures 3a and 3b (black lines). Fit equations: $8.6295E + 03 e^{-8.9052E - 03 \text{ alt}} + 2.8695E - 01 e^{9.2612E - 04 \text{ alt}}$ (Figure 3a) and $1.2945E + 16 e^{-3.5267E - 02 \text{ alt}} + 1.9204E + 01 e^{-1.5928E - 03 \text{ alt}}$ (b). INMS-derived mean positive ion masses are from a 2-D fit in SZA and altitude [Shebanits et al., 2013], except for T40 where the INMS measurements were used directly.

the CAPS/ELS negative ion data, which may shift the CAPS/ELS mass spectrum and therefore the mean mass slightly; this is currently under investigation but as the S/C potential is typically between -0.5 and -1.5 V, the correction is not expected to exceed 1V in Titan’s ionospheric environment and the subsequently slightly shifted mean ion mass would have minimal effects on the results.

3.3. Derivation of the Ion Charge Densities

The total ion charge densities are derived from the measured total ion current as follows. The approximation of a current to a spherical electrostatic probe moving in a plasma is [Fahleson et al., 1974]

$$I = \begin{cases} I_0(1 - \chi), & qU < 0 \\ I_0e^{-\chi}, & qU > 0 \end{cases}, \text{ where } I_0 = -4qn\pi r_p^2 \sqrt{\frac{v^2}{16} + \frac{k_b T}{2\pi m}} \text{ and } \chi = \frac{2q|U|}{mv^2 + 2k_b T} \quad (3)$$

For ions in Titan’s ionosphere the thermal energy term ($k_b T$) is much smaller [Shebanits et al., 2013] than the kinetic energy term (mv^2) and can therefore be neglected. Approximating the negative ion current as linear (with Taylor expansion) and setting $v \approx v_{sc}$ (using S/C ephemerides) we obtain equation (2). The total ion current to the probe is then (negative ions are indexed with “-” and positive with “+”):

$$I_{tot} = q_e \pi r_p^2 |v_{sc}| \sum_{ij} (Z_{i-} n_{i-} - n_{j+}) + \frac{2q_e^2 \pi r_p^2 |U|}{|v_{sc}|} \sum_{ij} \left(\frac{Z_{i-} n_{i-}}{m_{i-} / Z_{i-}} + \frac{n_{j+}}{m_{j+}} \right), \quad (4)$$

where \sum_{ij} denotes summing over ions (by masses), positive ions are assumed to be singly charged [Thissen et al., 2011] with $q_+ = q_e$ and negative ions have charge $q_- = -Z_- q_e$. Defining the effective masses of negative and positive ions as

$$\begin{cases} m_{\text{eff}-} = \left(\sum_i \frac{Z_i n'_i}{m_i} \right)^{-1} \\ m_{\text{eff}+} = \left(\sum_j \frac{n'_j}{m_j} \right)^{-1} \end{cases}, \quad (5)$$

where n'_{i-} and n'_{j+} are the relative abundances of ions (normalized to total density), we can rewrite the total ion current to the probe as

$$I_{\text{tot}} = q_e \pi r_{\text{lp}} |v_{\text{sc}}| (Z_- n_- - n_+) + \frac{2q_e^2 \pi r_{\text{lp}}}{|v_{\text{sc}}|} \left(\frac{Z_- n_-}{m_{\text{eff}-} / Z_-} + \frac{n_+}{m_{\text{eff}+}} \right) |U| = a - b|U|, \quad (6)$$

where $Z_- n_- = \sum_i Z_i n_{i-}$ and $n_+ = \sum_j n_{j+}$ are the total ion charge densities. The right-hand side is the defined linear fit to the measured ion current corrected for the photoelectron current and the S/C potential (comparison of the total ion currents to the RPWS/LP modeled using the mean ion mass and the effective ion mass is shown in Figure A1). The result is a system of equations:

$$\begin{cases} Z_- n_- - n_+ = \frac{a}{q_e \pi r_{\text{lp}} |v_{\text{sc}}|} = A \\ \frac{Z_- n_-}{m_{\text{eff}-} / Z_-} + \frac{n_+}{m_{\text{eff}+}} = -\frac{|v_{\text{sc}}| b}{q_e^2 \pi r_{\text{lp}}} = B \end{cases} \quad (7)$$

Solving for the total charge densities we obtain

$$\begin{cases} n_+ = \left(B \frac{m_{\text{eff}-}}{Z_-} - A \right) \left(\frac{m_{\text{eff}-}}{Z_- m_{\text{eff}+}} + 1 \right)^{-1} \\ Z_- n_- = \left(B m_{\text{eff}+} + A \right) \left(\frac{Z_- m_{\text{eff}+}}{m_{\text{eff}-}} + 1 \right)^{-1} \end{cases} \quad (8)$$

There are four measurement-derived variables that contain uncertainties. The parameters a and b have uncertainties from the fits to the RPWS/LP voltage-current characteristics. The effective masses (per charge) of positive and negative ions have uncertainties from the empirical fits to the INMS measurements and from the CAPS/IBS and CAPS/ELS measurements. Their respective total contributions to the uncertainties in the derived charge densities are $2\sigma_a \sim 10^{-12} \text{ cm}^{-3}$, $2\sigma_b \sim 10^{-8} \text{ cm}^{-3}$, and $2\sigma_{m_{\text{eff} \pm}} \sim 100 \text{ cm}^{-3}$. Together with the $\leq 50\%$ uncertainties of CAPS/ELS-derived mass/charge [Wellbrock *et al.*, 2013] this results in a total uncertainty in the positive and negative ion charge densities of $2\sigma \leq 400 \text{ cm}^{-3}$ or $\leq 20\%$ for the peak/maximum values. It should be noted, however, that the CAPS/ELS-derived densities represent an upper limit and the CAPS/ELS derived m_- may change as these quantities are likely sensitive to the MCP efficiency for the negative ions (currently under investigation).

3.4. Calculating the Charge of the Negative Ions/Dust Grains

The CAPS/ELS gives density/ q and mass/ q of the negative charge carriers. Since only the larger/heavier ions are likely to have more than one charge, there is no simple way to remove the dependency. For the RPWS/LP applications, mass/ q is an unknown variable (equation (2), last term) and there is no need to disentangle it. Using the CAPS/ELS-derived negative ion density/ q and the RPWS/LP negative ion charge density allows for a straight-forward way to empirically estimate the mean negative ion charge as

$$Z_- = \sqrt{\frac{Z_- N_{\text{-RPWS/LP}}}{N_{\text{-CAPS/ELS}}}}, \quad (9)$$

where the RPWS/LP- and CAPS/ELS-derived densities are marked accordingly. Note that this method does not discriminate between the negative charge carriers (ions or dust particles) although their respective mean mass depends on altitude (Figure 3d).

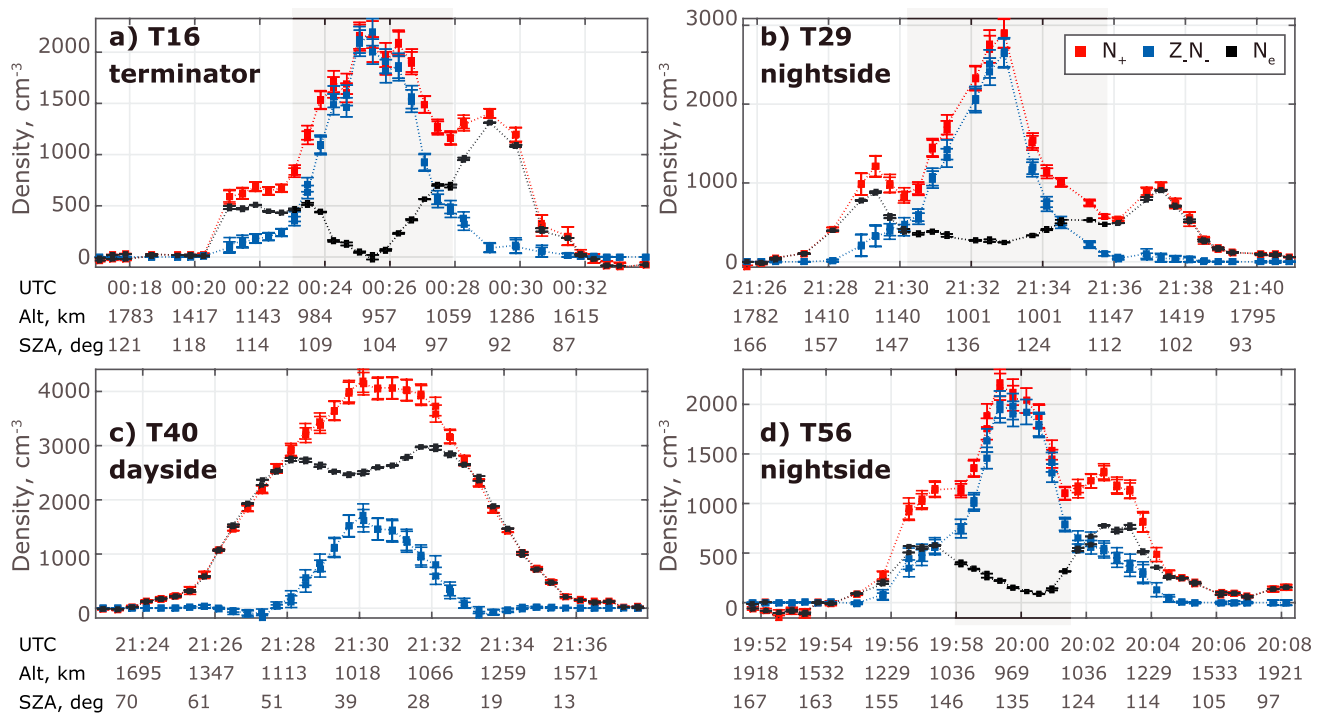


Figure 4. Positive (red) and negative (blue) ion charge densities derived from RPWS/LP with the new analysis method (every point is a “twin”, one is from -4 to 0 sweep and one from 0 to -4). The error bars represent the combined uncertainty (95% confidence intervals) from fitting the RPWS/LP characteristic and the effective ion mass. The electron densities are derived from the ion current assuming quasineutrality ($n_e + Z_- n_- = n_+$, first term in equation (6) with $2\sigma_a \sim 10^{-5} \text{ cm}^{-3}$). The shaded areas mark the regions of dusty plasma.

3.5. RPWS/LP Ion Current Modeling

The modeling of the RPWS/LP ion current response is performed in two steps. The necessary charge densities of positive and negative ions are first derived from the RPWS/LP ion analysis according to equation (7), using the respective mean ion mass and the effective ion mass. With the derived charge densities, the currents are then calculated by using the CAPS mass spectra and cross referenced with the measured ion current and the corresponding linear fit. An example of model output is shown in Figure A1.

4. Results and Discussion

The ion current model reconstructs the measurements very well (Figure A1), both OML theory and Fahleson approximation, below 1400 km altitude. This verifies the robustness of the Fahleson approximation for dense plasma applications (within the assumptions stated above) even in a presence of highly diverse ion populations.

4.1. Mean Ion Mass Profiles

The mean ion mass profiles derived with combined INMS and CAPS data (Figure 3) are valid for all flybys. There is an apparent invariability between night and day with regard to the altitude profiles of the mean ion mass, which may be attributed to the low number of included flybys. However, such invariability is not unexpected as it may be explained by the idea that the long-lived ions are transported from dayside to nightside ionosphere and cause a homogenous chemical composition [Cui *et al.*, 2009, 2010]; an order of magnitude estimate of the lifetime of heavy ions in an ion-ion plasma can be obtained by inverting the product of the ion-ion recombination rate coefficient ($\sim 10^{-7} \text{ cm}^3 \text{ s}^{-1}$, Vigen *et al.*, 2014) with the charge density ($\sim 1000 \text{ cm}^{-3}$), which gives an average heavy ion lifetime on the order of 10^4 s . It should also be noted that the invariability cannot be explained by the geometries of the included flybys: T29 and T56 are both between 20 h and 24 h Titan local time but in different hemispheres (T29 is in the northern and T56 is in the southern), T16 passes through the northern polar region from nightside into dusk and T40 is mostly in the southern hemisphere close to the equator passing from dusk to midday. This is an interesting topic to investigate in future studies as the INMS measurements indicate an increase in mean positive ion mass with SZA [Shebanits *et al.*, 2013].

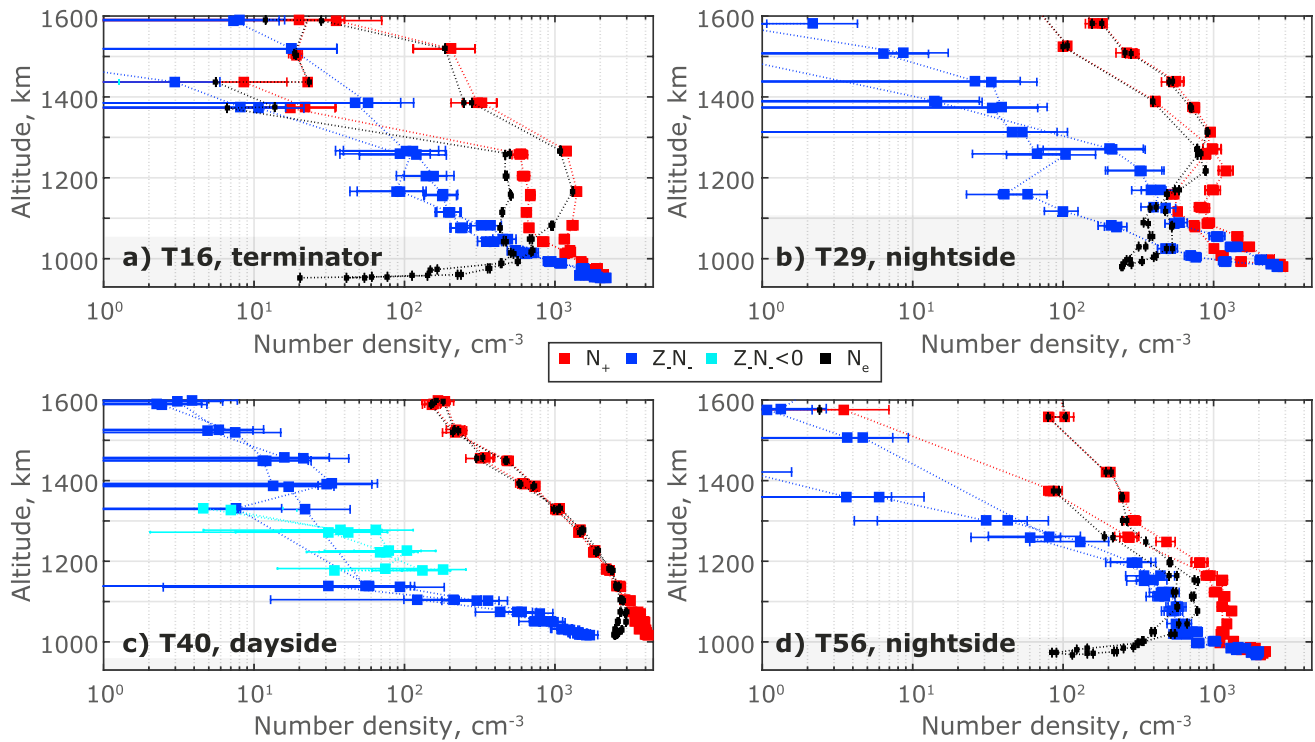


Figure 5. Same as Figure 4 but plotted in altitude (log scale). The cyan dots are the negative values of Z_{n-} (possibly due to ion drifts). The shaded areas mark the regions with dusty plasma (depleted electron densities, proposed region in case of T40, see also Figure 7).

4.2. Ion Charge Densities

The densities of positive ions and charge densities of negative ions inferred with the presented analysis method are plotted versus time in Figure 4. The sharp increase in ion charge densities at ~1000 km altitude in the terminator and nightside ionosphere is emphasized by plotting the same data versus altitude (Figure 5). Nightside flybys have ionospheric peaks of 950 cm^{-3} (1200 cm^{-3} outbound) at 1300 km (1200 km outbound) (T29) and 1150 cm^{-3} (1300 cm^{-3} outbound) at 1100 km (T56) sustained by the impacts of energetic particles (T16 and T29 are in the magnetospheric ram region) and possibly transport from the dayside ionosphere [Ågren et al., 2007, 2009; Cui et al., 2010; Richard et al., 2015]. The same processes are responsible for the inbound peak of T16, which is still in the nightside ($\text{SZA} > 110^\circ$), but the outbound peak is in the terminator region ($\text{SZA} \sim 90^\circ$) where the solar EUV is the major ionization source [Ågren et al., 2009; Shebanits et al., 2013; Richard et al., 2015], which explains the significantly higher positive ion densities there. Scale heights associated with the measured density profiles are presented in Table 1. The scale heights range between ~50 and ~250 km for both positive ions and negative charge carriers, ~160 km in the topside ionosphere (above ~1200 km). It is tempting to use the scale height to estimate the plasma temperatures with the hydrostatic equilibrium equation [Evans, 1965; McInnes, 1968]:

Table 1. Scale Heights Derived From the Measured Density Profiles (Figure 5)

	Flyby	Altitude (km)	Scale Height (km)	Lower Limit (95% conf.)	Upper Limit (95% conf.)
Positive ions	T16	950–1550	128–145	99	267
	T29	950–1600	124–131	90	237
	T40	1000–1600	141–252	132	263
	T56	965–1600	56–202	42	246
Negative ions/charge carriers	T16	950–1300	57–194	53	327
	T29	950–1300	57–193	67	303
	T40	950–1100	38–56	30	65
	T56	100–1200	229	193	283

$$H_p = \frac{T_e + T_i}{T'_e + T'_i + m_i g / k_B}, \quad (10)$$

where H_p is the plasma scale height, T_i and T_e are the ion and electron temperatures (T' is the altitude gradient), m_i is the mean ion mass, and g is the local gravitational acceleration. However, the hydrostatic equilibrium assumption breaks down in the topside ionosphere due to vertical plasma outflow [Cui *et al.*, 2010] and below ~ 1300 km altitude due to collisions with neutrals [Rosenqvist *et al.*, 2009]. Still, with the hydrostatic equilibrium assumption as a rough estimate and RPWS/LP-derived T_e profile [Edberg *et al.*, 2010], the resulting positive ion temperatures are within factor 2 of the estimates based on the CAPS/IBS and INMS measurements [Crory *et al.*, 2009] for the altitudes between 1300 and 1500 km. The negative ions and dust grains are present at altitudes below ~ 1200 km where the chemical processes are dominant, and therefore, the hydrostatic equilibrium does not apply.

The high densities of ion-ion (and dusty) plasma (sharp increases at ~ 1000 km altitude; Figure 5) imply severe differences between the effective rate coefficients for ion-electron and ion-ion neutralization processes, the former exceeding the latter possibly by a factor of ~ 5 or more, indicating that positive ions become longer-lived in electron-depleted regions such as ion-ion and dusty plasmas [Vigren *et al.*, 2014]. Previously, ion-ion or dusty plasma has been detected during the T70 flyby [Ågren *et al.*, 2012] and on the nightside of Titan's ionosphere below 1000 km altitude [Shebanits *et al.*, 2013]. With the presented method we can extend this region to include the terminator region (T16), although at seemingly lower altitudes (≈ 960 km for T16). This, together with the low ion-ion recombination rates, the observed electron depletion, and the fact that the peak in the negative ion charge densities is rarely detected on the dayside by the RPWS/LP down to the minimum altitude (950 km) reached in this region by the Cassini S/C, suggests that the dusty plasma may also be present on the dayside at altitudes below 900 km and is therefore a global phenomenon in Titan's ionosphere.

For T40, the charge density of negative ions is derived as negative at the altitudes 1150–1350 km. We interpret this as a possible indicator of ion drifts: the ions are assumed stationary; deviations from v_{sc} by $\sim 250 \text{ ms}^{-1}$ [Müller-Wodarg *et al.*, 2008; Crory *et al.*, 2009] are estimated to shift the ion densities by $\sim 10\%$ of the total ion density (equations (7) and (8)); for T40 at 1150–1350 km this is $\sim 200 \text{ cm}^{-3}$, which matches the shift in the negative ion charge densities.

4.3. Negative Ion/Dust Grain Charge

We present the first empirical estimate of the mean negative ion charge (Figure 6a). The negative ions have the average charge of $-2.5q_e \leq Z_- \leq -1.5q_e$ (q_e is the elementary charge), with an exponential trend inversely proportional to altitude, suggesting a significant number of the doubly and triply charged negative particles below ~ 1000 km altitude. This estimate of Z_- is also in agreement with theoretical predictions [Shebanits *et al.*, 2013] based on the thermal equilibrium of the ionospheric plasma and was used in the modeled ion currents. Assuming thermal equilibrium, spherical grains and using the Cassini S/C potential (U_{sc}) as a proxy for the dust grain potential [Whipple *et al.*, 1985; Goertz, 1989; Horányi *et al.*, 2004; Hill *et al.*, 2012; Engelhardt *et al.*, 2015] allow one to calculate the apparent average dust grain radius R_D needed to accommodate the charge Z_-q_e :

$$R_D = \frac{Z_-q_e}{4\pi\epsilon_0 U_{sc}}, \quad (11)$$

where ϵ_0 is the vacuum permittivity. The resulting R_D is between 2 and 8 nm (Figure 6b). This is in agreement with models based on the CAPS/ELS data [Michael *et al.*, 2011]. The validity of the dust grain potential approximation by U_{sc} was tested by Engelhardt *et al.* [2015] in the much denser dusty plasma of Enceladus' plume; the authors have shown that the contribution of other charging mechanisms than the thermal equilibrium is not significant. The approximation is therefore also valid for the average dust grain in Titan's ionosphere; it should be noted, however, that some charge fluctuations are expected for the individual nanometer-sized grains [Horányi *et al.*, 2004].

There is no statistically significant difference in negative ion charge between dayside (T40, orange in Figure 6a), nightside (T29 in green and T56 in red) and terminator (T16 in blue) ionosphere. This can (again) be attributed to the low number of flybys included in the study. Still, there are a few points to note. Dayside (T40) Z_- is expected to be lower at higher altitudes (above ~ 1100 km) due to photoemission of electrons and the fact that the ion population is dominated by lighter positive ions (compared to lower altitudes; Figure 3). There

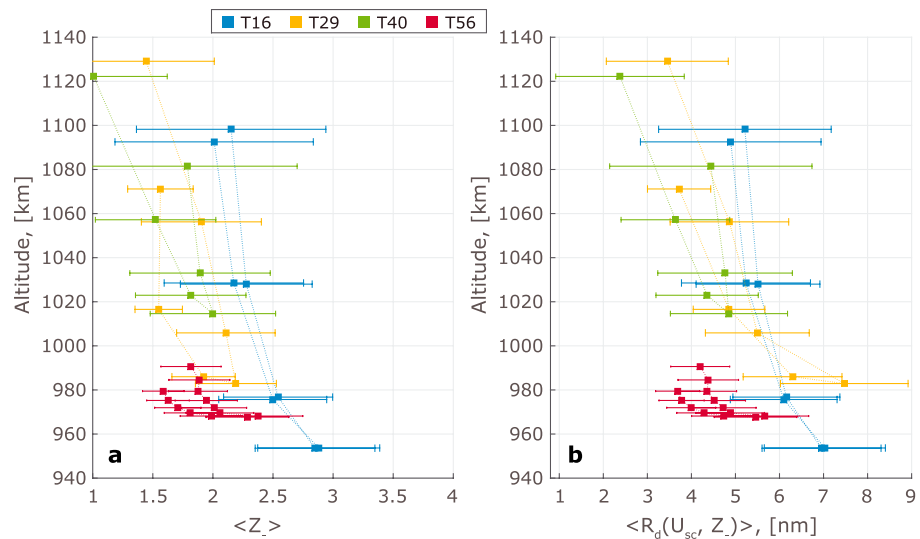


Figure 6. Altitude plots: (a) average negative ion/dust grain charge (Z_n) derived from CAPS/ELS and RPWS/LP measurements; (b) apparent average dust radius derived from Z_n and dust potential ($\approx U_{sc}$). The four flybys are color-coded; the error bars represent the combined uncertainty (95% confidence).

is only a single data point to support this, however, and analysis of other dayside flybys is required. Below ~ 1100 km altitude the photoionization declines and the dayside/nightside dust grain charge is expected to be similar. The inverse dependency of the ion-ion recombination rates on the ion masses [Vigren *et al.*, 2014] can also explain the presence of the doubly and triply charged negative charge carriers and the overall exponential trend of Z_- with decreasing altitude since the mean ion mass of both positive and negative ions increases likewise exponentially toward lower altitudes. Another feature that stands out is that Z_- at the terminator flyby (T16) is a factor ~ 0.5 more negative than the rest. Coincidentally, the largest negatively charged dust grains were detected during T16 [Coates *et al.*, 2007]. Moreover, most of the terminator flybys are close to the northern region of Titan's ionosphere where the magnetospheric particles (electrons especially) are expected to enter the ionosphere, T16 in particular is right above Titan's north pole ($>85^\circ$ north latitude). However, this difference is within 2 standard deviations and more flybys need to be studied to draw definite conclusions.

We may adapt the methods for collisional charging of conducting spherical grains [Draine and Sutin, 1987; Meyer-Vernet, 2013] to estimate the requirements for the dust particles to have a charge of $-2q_e$. Given $T_e \sim 500$ K, $n_e/n_i = 0.1$, and a positive ion mass $m_+ \approx 100$ amu, the R_d required for the charge equilibrium is ~ 19.5 nm for $Z_- = -2$ and 6.5 nm for $Z_- = -1$ (for the above we assumed $T_i = T_e$, lower values of T_i would tend to slightly enhance the required radii). In view of this theoretical framework, the observationally derived $Z_- \approx -2$ is surprisingly low. The specified theory rather suggests a near absence of doubly negatively charged dust grains in the mass range of 500–2000 amu. The fact that we here have applied a theory ideal for conducting macromolecules is unlikely to explain the discrepancy. However, the spherical grain assumption may not be valid as the mass densities of spherical particles with $R_d \sim 2 - 8$ nm and the mass measured by the CAPS/ELS are $\sim 1-6$ kg m^{-3} , which fits hollow structures such as fractal particles [Sittler *et al.*, 2009; Waite *et al.*, 2009; Michael *et al.*, 2011]. Michael *et al.* [2011] also estimates R_d to be <10 nm and the grains to be singly charged based on the CAPS/ELS measurements. The effect of the dust grain shape on its charge state requires sophisticated theory, well beyond the scope of the present study. Another argument for singly charged negative grains is that the CAPS/ELS spectra are often smooth above ~ 100 amu/charge, whereas multiple charges should show up as extra peaks; i.e., a doubly charged 1000 amu/charge population should be accompanied by a 2000 amu/charge peak for the singly charged grains of the same mass [Hill *et al.*, 2012], but more studies are needed to investigate this in Titan's ionosphere. It should also be noted that since the CAPS/ELS-derived densities represent the upper limit, the presented average negative ion/dust grain charge numbers are likely to be a lower limit.

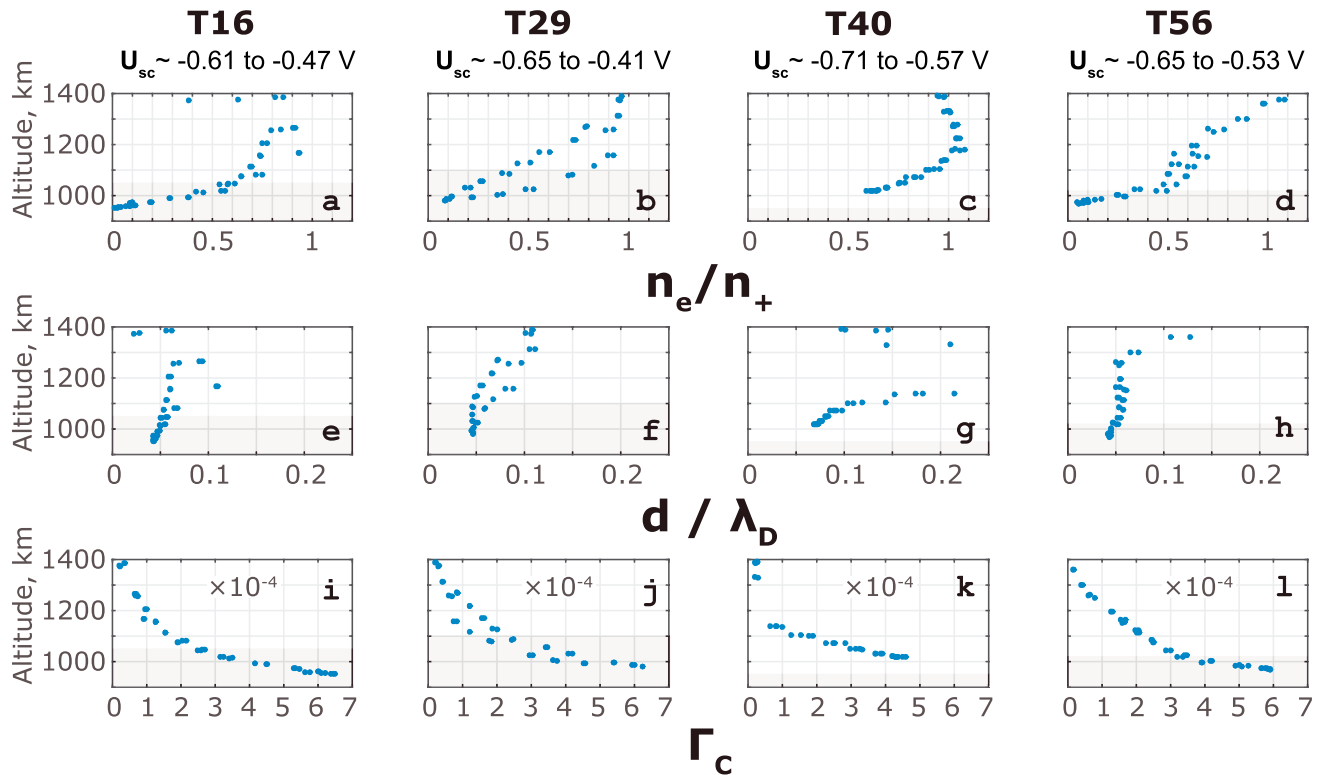


Figure 7. Dusty plasma characteristics: (a–d) electron to positive ion number density ratio, (e–h) dust intergrain distance to Debye length ratio, and (i–l) Coulomb coupling parameter. Specified U_{sc} are typical values for each flyby (proxy for dust grain potential). The electron densities are derived from the ion current assuming quasineutrality in the same way as in Figure 5. The shaded areas mark the regions with dusty plasma (proposed region in case of T40).

4.4. Dusty Plasma

The ratio of the dust Debye length λ_D to the intergrain distance is ≥ 2 for T40 and ≥ 10 for T16, T29, and T56 (Figures 7e–7h). Together with the depletion of electrons (Figures 7a–7d) this identifies the presence of dust below 1100 km altitude (grey-shaded). The apparent average dust grain radius R_D is estimated to be 2–8 nm (Figure 6b). The intergrain distance is $d \geq 0.1$ cm, estimated as the inverse cubic root of the measured charge density of the negative charge carriers. The dusty plasma condition $R_D \ll d < \lambda_D$ [Shukla and Mamun, 2002; Morooka et al., 2011; Shafiq et al., 2011] is therefore fulfilled throughout the ionosphere of Titan, down to the lowest in situ observable altitudes. The maximum positive and negative ion densities for the terminator and nightside flybys are measured below 1100 km altitude (Figure 5), where the ionosphere is depleted of electrons and behaves as a dusty plasma [Shebanits et al., 2013] according to Shukla’s definition. The collective behavior of the dusty plasma is characterized by the Coulomb coupling parameter (Γ_C), a ratio of the potential and thermal energies of the dust grains. For the selected flybys $\Gamma_C \sim 10^{-4}$ (Figures 7i–7l), indicating a weakly coupled plasma (ν is described in more details in the Appendix).

The dusty plasma condition ($R_D \ll d < \lambda_D$) is fulfilled below 1400 km throughout Titan’s ionosphere. This implies that as the negative ions grow to the size of dust grains (~ 1 nm, ~ 1000 amu), the ionospheric plasma becomes dusty and the dust exhibits weakly collective behavior (Coulomb coupling parameter $\Gamma_C \sim 10^{-4}$, see Appendix). At altitudes below 900–1000 km, collisions with neutrals may disrupt the collective behavior of the dust as the collective oscillations of the plasma particles will be dampened by the relatively stationary neutrals [Shukla and Mamun, 2002]. Therefore, the influence of the collisions with neutrals can be checked by comparing the ion plasma frequencies to the dust-neutral collision frequency. The latter can be approximated by the ion-neutral collision frequency, which reaches ~ 10 s $^{-1}$ at 1000 km [Rosenqvist et al., 2009]. The ion plasma frequencies ($\omega_{p\pm} = N_{\pm}^{0.5} Z_{\pm} q_e \epsilon_0^{-0.5} m_{\pm}^{-0.5}$) are much higher, however, ~ 1 kHz for positive ions and ~ 0.3 kHz for the negative dust grains, confirming the collective behavior of the observed dusty plasma. Observation of such a collective behavior with the Cassini RPWS is very difficult as the reaction wheels on the Cassini S/C create interferences at the frequencies of interest (< 1 kHz).

5. Conclusions

1. We have developed a method for detailed analysis of the current-voltage characteristic for negative bias potentials of the RPWS/LP, adapted for Titan's ionosphere.
2. Mean ion mass profiles derived with INMS are empirically extended to include heavier ions, applicable to all Titan flybys. The absence of obvious day-night variability in the mean ion masses at 900–1400 km altitudes may be explained by the ion transport (dayside to nightside) ionosphere in this layer.
3. Electrons are depleted in the nightside and terminator ionosphere at altitudes below ν km and expected to be depleted in the dayside ionosphere below 900 km; we therefore conclude that ion-ion plasma is present on Titan in these regions and possibly in the dayside ionosphere as well below 900 km, with heavy negative ions as dominant negative charge carriers.
4. Titan's ionosphere has two main peaks below 1400 km altitude: the upper, due to ionization by the primary source (solar EUV on the dayside and magnetospheric particles on the nightside), and the lower, due to the formation of the heavy dust particles. The altitudes of the lower peaks are not observed for the included flybys; maximum charge densities measured are ≥ 2 times higher than the primary peaks.
5. The dusty plasma condition is fulfilled below at least 1400 km altitude throughout the ionosphere of Titan; weakly coupled nanometer-sized dust particles are detected below 1100 km down to the lowest altitude reached by the Cassini S/C.
6. We present the first empirical estimate of the average negative ion/dust grain charge with values between -2.5 and -1.5 elementary charges. The average charge increases exponentially with decreasing altitude, suggesting a significant amount of doubly and triply charged negative charge carriers at altitudes below 1000 km.

Appendix A

Derivation of the OML Ion Current

Starting with the total current to the probe expression from Engwall [2006, equation (3.26) (plasma drift velocity v_d is in our case the S/C velocity v_{sc}):

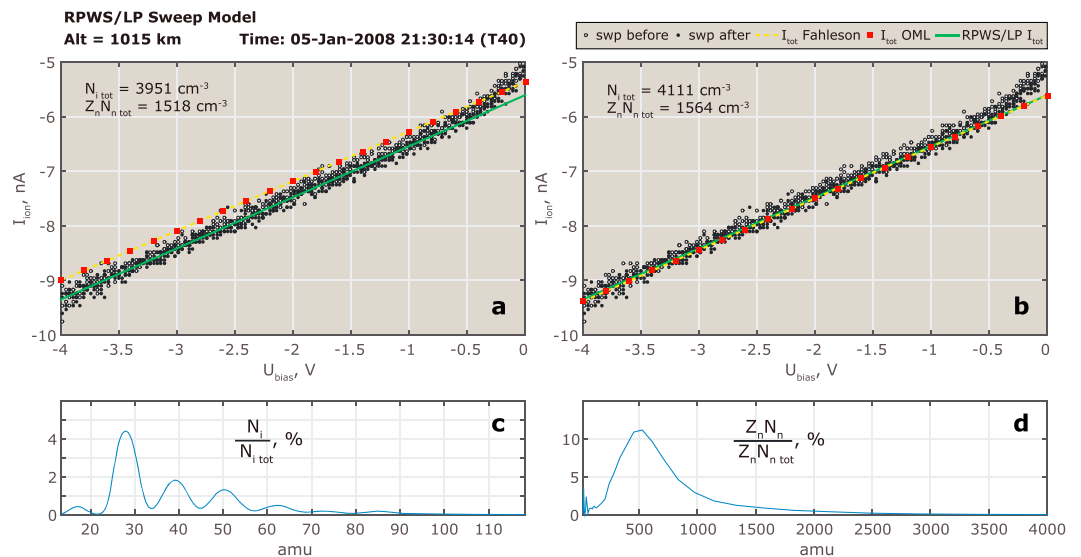


Figure A1. Example of comparison between the measured and the modeled total ion current to the RPWS/LP: (a) using the mean ion mass (heavy ions included) and (b) using the effective ion mass for the derivation of the specified charge densities. I_{tot} OML (red squares) is the current calculated with equation (1); I_{tot} Fahleson (black dashed line) is the current calculated with equation (2). The closest (in time) RPWS/LP sweeps to the CAPS spectra are plotted in the background for comparison: preceding (empty circles) and succeeding (filled circles). The green line is the fit to RPWS/LP sweeps. All data are interpolated to match the CAPS/ELS time stamp. Bottom figures show the (c) CAPS/IBS and (d) CAPS/ELS mass spectra, used as input for the model; the y axis is the abundance in % (normalized to respective total density).

$$I = qnr_{ip}^2 \sqrt{\frac{2\pi k_B T}{m}} \left[e^{-\frac{m}{2k_B T}(v_1^2 + v_{sc}^2)} \left(\frac{v_1}{v_{sc}} \sinh\left(\frac{mv_{sc}v_1}{k_B T}\right) + \cosh\left(\frac{mv_{sc}v_1}{k_B T}\right) \right) + \sqrt{\frac{k_B T}{2mv_{sc}^2}} \left(\frac{mv_{sc}^2}{k_B T} + 1 - \frac{2qU}{k_B T} \right) E\left(\sqrt{\frac{m}{2k_B T}}(v_1 - v_{sc}), \sqrt{\frac{m}{2k_B T}}(v_1 + v_{sc})\right) \right] \quad (A1)$$

where $E(x_1, x_2) = \int_{x_1}^{x_2} e^{-y^2} dy$ is the error function. Note that there is a typo in *Engwall* [2006, equation (3.26): $I = qna \dots$ should be $I = qna^2 \dots$ (a is the probe radius, r_{ip}).

Switching to the general definition of the error function, $\text{erf}(x) = \frac{2}{\sqrt{\pi}} \int_0^x e^{-y^2} dy$ and substituting $\sinh x = \frac{e^x - e^{-x}}{2}$ and $\cosh x = \frac{e^x + e^{-x}}{2}$, we get

$$I = qnr_{ip}^2 \sqrt{\frac{2\pi k_B T}{m}} \left[e^{-\frac{m}{2k_B T}(v_1^2 + v_{sc}^2)} \frac{1}{2} \left(\frac{v_1}{v_{sc}} \left(e^{\frac{mv_{sc}v_1}{k_B T}} - e^{-\frac{mv_{sc}v_1}{k_B T}} \right) + e^{\frac{mv_{sc}v_1}{k_B T}} + e^{-\frac{mv_{sc}v_1}{k_B T}} \right) + \sqrt{\frac{k_B T}{2mv_{sc}^2}} \left(\frac{mv_{sc}^2}{k_B T} + 1 - \frac{2qU}{k_B T} \right) \frac{\sqrt{\pi}}{2} (\text{erf}(A) - \text{erf}(B)) \right] \quad (A2)$$

where $A = \sqrt{\frac{m}{2k_B T}}(v_1 + v_{sc})$ and $B = \sqrt{\frac{m}{2k_B T}}(v_1 - v_{sc})$.

Multiplying the exponential terms yields

$$I = qnr_{ip}^2 \sqrt{\frac{2\pi k_B T}{m}} \left[\frac{1}{2} \left(\frac{v_1}{v_{sc}} \left(e^{-\frac{m}{2k_B T}(v_1^2 + v_{sc}^2) + \frac{mv_{sc}v_1}{k_B T}} - e^{-\frac{m}{2k_B T}(v_1^2 + v_{sc}^2) - \frac{mv_{sc}v_1}{k_B T}} \right) + e^{-\frac{m}{2k_B T}(v_1^2 + v_{sc}^2) + \frac{mv_{sc}v_1}{k_B T}} + e^{-\frac{m}{2k_B T}(v_1^2 + v_{sc}^2) - \frac{mv_{sc}v_1}{k_B T}} \right) + \sqrt{\frac{k_B T}{2mv_{sc}^2}} \left(\frac{mv_{sc}^2}{k_B T} + 1 - \frac{2qU}{k_B T} \right) \frac{\sqrt{\pi}}{2} (\text{erf}(A) - \text{erf}(B)) \right] \quad (A3)$$

The exponential powers can now be rewritten as

$$-\frac{m}{2k_B T}(v_1^2 + v_{sc}^2) + \frac{mv_{sc}v_1}{k_B T} = -\frac{m}{2k_B T}(v_1^2 + v_{sc}^2 - 2v_1v_{sc}) = -\frac{m}{k_B T}(v_1 - v_{sc})^2 = -B^2 \quad (A4)$$

and similarly

$$-\frac{m}{2k_B T}(v_1^2 + v_{sc}^2) - \frac{mv_{sc}v_1}{k_B T} = -\frac{m}{k_B T}(v_1 + v_{sc})^2 = -A^2 \quad (A5)$$

Grouping the exponential terms and extracting the $\frac{1}{2}$ from the square brackets, we arrive at equation (1):

$$I = qnr_{ip}^2 \sqrt{\frac{\pi k_B T}{2m}} \left[\left(e^{-A^2} \left(1 - \frac{v_1}{v_{sc}} \right) + e^{-B^2} \left(1 + \frac{v_1}{v_{sc}} \right) \right) + \sqrt{\frac{\pi k_B T}{2mv_{sc}^2}} \left(\frac{mv_{sc}^2}{k_B T} + 1 - \frac{2qU}{k_B T} \right) (\text{erf}(A) - \text{erf}(B)) \right] \quad (A6)$$

Dusty Plasma Parameters

Dust Debye length is calculated assuming local thermodynamic equilibrium [Shukla, 2001]:

$$\lambda_D = \frac{\lambda_{De} \lambda_{D+}}{\sqrt{\lambda_{De}^2 + \lambda_{D+}^2}} \quad (A7)$$

where λ_{De} and λ_{D+} are the electron and positive ion Debye lengths, respectively.

Coupling of plasma is characterized by the ratio of the potential and thermal energies of the dust grains—Coulomb coupling parameter Γ_C :

$$\Gamma_C = \frac{Z_- q_e^2}{4\pi\epsilon_0 d k_B T_D} \exp\left(-\frac{d}{\lambda_D}\right) \quad (A8)$$

where Z_- is the dust grain charge number, q_e is the elementary charge, d is the intergrain distance, and T_D is

the dust temperature. The exponential term represents the shielding effect. Dusty plasma is strongly coupled when $\Gamma_C \gg 1$ and weakly coupled when $\Gamma_C \ll 1$ [Shukla, 2001].

Ion Current Response

Below are examples of the RPWS/LP ion current modeling using the mean ion mass to derive the densities compared to the effective ion mass (Figure A1), to illustrate the improvement in the reproduced ion current.

Acknowledgments

The authors acknowledge funding and RPWS/LP instrument support by the Swedish National Space Board, and the Cassini project support by NASA. K.M. acknowledges support from NASA grant NNX13AQ99G. N.J.T.E. acknowledges funding by the Swedish National Space Board under contract Dnr 135/13 and by Vetenskapsrådet under contract 621-2013-4191. The data used in this paper are included in the figures and listed in the references.

References

- Ågren, K., et al. (2007), On magnetospheric electron impact ionisation and dynamics in Titan's ram-side and polar ionosphere—A Cassini case study, *Ann. Geophys.*, *25*(11), 2359–2369, doi:10.5194/angeo-25-2359-2007.
- Ågren, K., J. E. Wahlund, P. Garnier, R. Modolo, J. Cui, M. Galand, and I. Müller-Wodarg (2009), On the ionospheric structure of Titan, *Planet. Space Sci.*, *57*(14–15), 1821–1827, doi:10.1016/j.pss.2009.04.012.
- Ågren, K., N. J. T. Edberg, and J.-E. Wahlund (2012), Detection of negative ions in the deep ionosphere of Titan during the Cassini T70 flyby, *Geophys. Res. Lett.*, *39*, L120201, doi:10.1029/2012GL051714.
- Bird, M.-K., R. Dutta-Roy, S.-W. Asmar, and T.-A. Rebold (1997), Detection of Titan's ionosphere from Voyager 1 radio occultation observations, *Icarus*, *130*(2), 426–436, doi:10.1006/icar.1997.5831.
- Coates, A. J., F. J. Crary, G. R. Lewis, D. T. Young, J. H. Waite, and E. C. Sittler (2007), Discovery of heavy negative ions in Titan's ionosphere, *Geophys. Res. Lett.*, *34*, L22103, doi:10.1029/2007GL030978.
- Coates, A. J., A. Wellbrock, G. R. Lewis, G. H. Jones, D. T. Young, F. J. Crary, and J. H. Waite (2009), Heavy negative ions in Titan's ionosphere: Altitude and latitude dependence, *Planet. Space Sci.*, *57*(14–15), 1866–1871, doi:10.1016/j.pss.2009.05.009.
- Coates, A. J., A. Wellbrock, G. R. Lewis, G. H. Jones, D. T. Young, F. J. Crary, J. H. Waite, R. E. Johnson, T. W. Hill, and E. C. Sittler Jr. (2010), Negative ions at Titan and Enceladus: Recent results, *Faraday Discuss.*, *147*, 293, doi:10.1039/c004700g.
- Crory, F. J., B. A. Magee, K. Mandt, J. H. Waite, J. Westlake, and D. T. Young (2009), Heavy ions, temperatures and winds in Titan's ionosphere: Combined Cassini CAPS and INMS observations, *Planet. Space Sci.*, *57*(14–15), 1847–1856, doi:10.1016/j.pss.2009.09.006.
- Cravens, T. E. (2005), Titan's ionosphere: Model comparisons with Cassini Ta data, *Geophys. Res. Lett.*, *32*, L12108, doi:10.1029/2005GL023249.
- Cravens, T. E., et al. (2006), Composition of Titan's ionosphere, *Geophys. Res. Lett.*, *33*, L07105, doi:10.1029/2005GL025575.
- Cravens, T. E., et al. (2009), Model-data comparisons for Titan's nightside ionosphere, *Icarus*, *199*(1), 174–188, doi:10.1016/j.icarus.2008.09.005.
- Cui, J., M. Galand, R. V. Yelle, V. Vuitton, J.-E. Wahlund, P. P. Lavvas, I. C. F. Müller-Wodarg, T. E. Cravens, W. T. Kasprzak, and J. H. Waite (2009), Diurnal variations of Titan's ionosphere, *J. Geophys. Res.*, *114*, A06310, doi:10.1029/2009JA014228.
- Cui, J., M. Galand, R. V. Yelle, J.-E. Wahlund, K. Ågren, J. H. Waite, and M. K. Dougherty (2010), Ion transport in Titan's upper atmosphere, *J. Geophys. Res.*, *115*, A06314, doi:10.1029/2009JA014563.
- Draine, B. T., and B. Sutin (1987), Collisional charging of interstellar grains, *Astrophys. J.*, *320*, 803, doi:10.1086/165596.
- Edberg, N. J. T., J.-E. Wahlund, K. Ågren, M. W. Morooka, R. Modolo, C. Bertucci, and M. K. Dougherty (2010), Electron density and temperature measurements in the cold plasma environment of Titan: Implications for atmospheric escape, *Geophys. Res. Lett.*, *37*, L20105, doi:10.1029/2010GL044544.
- Edberg, N. J. T., K. Ågren, J.-E. Wahlund, M. W. Morooka, D. J. Andrews, S. W. H. Cowley, A. Wellbrock, A. J. Coates, C. Bertucci, and M. K. Dougherty (2011), Structured ionospheric outflow during the Cassini T55–T59 Titan flybys, *Planet. Space Sci.*, *59*(8), 788–797, doi:10.1016/j.pss.2011.03.007.
- Edberg, N. J. T., et al. (2015), Effects of Saturn's magnetospheric dynamics on Titan's ionosphere, *J. Geophys. Res. Space Physics*, *120*, 8884–8898, doi:10.1002/2015JA021373.
- Engelhardt, I. A. D., J.-E. Wahlund, D. J. Andrews, A. I. Eriksson, S. Ye, W. S. Kurth, D. A. Gurnett, M. W. Morooka, W. M. Farrell, and M. K. Dougherty (2015), Plasma regions, charged dust and field-aligned currents near Enceladus, *Planet. Space Sci.*, *117*, 453–469, doi:10.1016/j.pss.2015.09.010.
- Engwall, E. (2006), Cold magnetospheric plasma flows: Properties and interaction with spacecraft, Uppsala Univ., Sweden.
- Evans, J. V. (1965), Cause of the mid-latitude evening increase in f_oF_2 , *J. Geophys. Res.*, *70*, 1175–1185, doi:10.1029/JZ070i005p01175.
- Fahleson, U., C.-G. Fälthammar, and A. Pedersen (1974), Ionospheric temperature and density measurements by means of spherical double probes, *Planet. Space Sci.*, *22*(1), 41–66, doi:10.1016/0032-0633(74)90122-6.
- Galand, M., A. J. Coates, T. E. Cravens, and J.-E. Wahlund (2014), Titan's ionosphere, in *Titan*, edited by I. Müller-Wodarg, C. A. Griffith, et al., pp. 376–418, Cambridge Univ. Press, Cambridge.
- Goertz, C. K. (1989), Dusty plasmas in the solar system, *Rev. Geophys.*, *27*, 271, doi:10.1029/RG027i002p00271.
- Gudipati, M. S., R. Jacovi, I. Couturier-Tamburelli, A. Lignell, and M. Allen (2013), Photochemical activity of Titan's low-altitude condensed haze, *Nat. Commun.*, *4*, 1648, doi:10.1038/ncomms2649.
- Gurnett, D. A., et al. (2004), The Cassini radio and plasma wave investigation, *Space Sci. Rev.*, *114*(1–4), 395–463, doi:10.1007/s11214-004-1434-0.
- Hill, T. W., et al. (2012), Charged nanograins in the Enceladus plume, *J. Geophys. Res.*, *117*, A05209, doi:10.1029/2011JA017218.
- Horányi, M., T.-W. W. Hartquist, O. Havnes, D.-A. A. Mendis, and G.-E. E. Morfill (2004), Dusty plasma effects in Saturn's magnetosphere, *Reviews*, *42*(4), 1–20, doi:10.1029/2004RG000151.1.
- Laframboise, J. G., and L. W. Parker (1973), Probe design for orbit-limited current collection, *Phys. Fluids*, *16*(5), 629, doi:10.1063/1.1694398.
- Lavvas, P., et al. (2013), Aerosol growth in Titan's ionosphere, *Proc. Natl. Acad. Sci. U.S.A.*, *110*(8), 2729–2734, doi:10.1073/pnas.1217059110.
- Lewis, G. R., N. André, C. S. Arridge, A. J. Coates, L. K. Gilbert, D. R. Linder, and A. M. Rymer (2008), Derivation of density and temperature from the Cassini-Huygens CAPS electron spectrometer, *Planet. Space Sci.*, *56*(7), 901–912, doi:10.1016/j.pss.2007.12.017.
- Linder, D. R., A. J. Coates, R. D. Woodliffe, C. Alsop, A. D. Johnstone, M. Grande, A. Preece, B. Narheim, and D. T. Young (1998), The Cassini CAPS Electron Spectrometer, pp. 257–262.
- Magee, B. A., J. H. Waite, K. E. Mandt, J. Westlake, J. Bell, and D. A. Gell (2009), INMS-derived composition of Titan's upper atmosphere: Analysis methods and model comparison, *Planet. Space Sci.*, *57*(14–15), 1895–1916, doi:10.1016/j.pss.2009.06.016.

- Mandt, K. E., et al. (2012), Ion densities and composition of Titan's upper atmosphere derived from the Cassini Ion Neutral Mass Spectrometer: Analysis methods and comparison of measured ion densities to photochemical model simulations, *J. Geophys. Res.*, *117*, E10006, doi:10.1029/2012je004139.
- McInnes, B. A. (1968), Variations of plasma scale height in the upper ionosphere during the sunrise period, *J. Geophys. Res.*, *73*, 5603–5613, doi:10.1029/JA073i017p05603.
- Medicus, G. (1962), Spherical Langmuir Probe in "drifting" and "accelerated" Maxwellian distribution, *J. Appl. Phys.*, *33*(10), 3094, doi:10.1063/1.1728574.
- Meyer-Vernet, N. (2013), On the charge of nanograins in cold environments and Enceladus dust, *Icarus*, *226*(1), 1–24, doi:10.1016/j.icarus.2013.06.014.
- Michael, M., S. N. Tripathi, P. Arya, A. Coates, A. Wellbrock, and D. T. Young (2011), High-altitude charged aerosols in the atmosphere of Titan, *Planet. Space Sci.*, *59*(9), 880–885, doi:10.1016/j.pss.2011.03.010.
- Morooka, M. W., J.-E. Wahlund, A. I. Eriksson, W. M. Farrell, D. A. Gurnett, W. S. Kurth, A. M. Persoon, M. Shafiq, M. André, and M. K. G. Holmberg (2011), Dusty plasma in the vicinity of Enceladus, *J. Geophys. Res.*, *116*, A12221, doi:10.1029/2011JA017038.
- Mott-Smith, H. M., and I. Langmuir (1926), The theory of collectors in gaseous discharges, *Phys. Rev.*, *28*(4), 727–763, doi:10.1103/PhysRev.28.727.
- Müller-Wodarg, I. C. F., R. V. Yelle, N. Borggren, and J. H. Waite (2006), Waves and horizontal structures in Titan's thermosphere, *J. Geophys. Res.*, *111*, A12315, doi:10.1029/2006JA011961.
- Müller-Wodarg, I. C. F., R. V. Yelle, J. Cui, and J. H. Waite (2008), Horizontal structures and dynamics of Titan's thermosphere, *J. Geophys. Res.*, *113*, E10005, doi:10.1029/2007JE003033.
- Niemann, H. B., et al. (2005), The abundances of constituents of Titan's atmosphere from the GCMS instrument on the Huygens probe, *Nature*, *438*(7069), 779–784, doi:10.1038/nature04122.
- Richard, M. S., T. E. Cravens, I. P. Robertson, J. H. Waite, J.-E. Wahlund, F. J. Cray, and A. J. Coates (2011), Energetics of Titan's ionosphere: Model comparisons with Cassini data, *J. Geophys. Res.*, *116*, A09310, doi:10.1029/2011JA016603.
- Richard, M. S., et al. (2015), An empirical approach to modeling ion production rates in Titan's ionosphere I: Ion production rates on the dayside and globally, *J. Geophys. Res. Space Physics*, *120*, 1281–1298, doi:10.1002/2014JA020343.
- Rosenqvist, L., J. E. Wahlund, K. Ågren, R. Modolo, H. J. Opgenoorth, D. Strobel, I. Müller-Wodarg, P. Garnier, and C. Bertucci (2009), Titan ionospheric conductivities from Cassini measurements, *Planet. Space Sci.*, *57*(14–15), 1828–1833, doi:10.1016/j.pss.2009.01.007.
- Shafiq, M., J.-E. Wahlund, M. W. Morooka, W. S. Kurth, and W. M. Farrell (2011), Characteristics of the dust–plasma interaction near Enceladus' South Pole, *Planet. Space Sci.*, *59*(1), 17–25, doi:10.1016/j.pss.2010.10.006.
- Shebanits, O., J.-E. Wahlund, K. Mandt, K. Ågren, N. J. T. Edberg, and J. H. Waite (2013), Negative ion densities in the ionosphere of Titan–Cassini RPWS/LP results, *Planet. Space Sci.*, *84*, 153–162, doi:10.1016/j.pss.2013.05.021.
- Shukla, P. K. (2001), A survey of dusty plasma physics, *Phys. Plasmas*, *8*(5), 1791, doi:10.1063/1.1343087.
- Shukla, P. K., and A. A. Mamun (2002), Introduction to dusty plasma physics, *Plasma Phys. Control. Fusion*, *44*(3), 395–395, doi:10.1088/0741-3335/44/3/701.
- Sittler, E. C., A. Ali, J. F. Cooper, R. E. Hartle, R. E. Johnson, A. J. Coates, and D. T. Young (2009), Heavy ion formation in Titan's ionosphere: Magnetospheric introduction of free oxygen and a source of Titan's aerosols? *Planet. Space Sci.*, *57*(13), 1547–1557, doi:10.1016/j.pss.2009.07.017.
- Thissen, R., O. Witasse, O. Dutuit, C. S. Wedlund, G. Gronoff, and J. Liliensten (2011), Doubly-charged ions in the planetary ionospheres: A review, *Phys. Chem. Chem. Phys.*, *13*(41), 18,264, doi:10.1039/c1cp21957j.
- Vigren, E., M. Galand, O. Shebanits, J.-E. Wahlund, W. D. Geppert, P. Lavvas, V. Vuitton, and R. V. Yelle (2014), Increasing positive ion number densities below the peak of ion–electron pair production in Titan's ionosphere, *Astrophys. J.*, *786*(1), 69, doi:10.1088/0004-637X/786/1/69.
- Vigren, E., et al. (2015), Ionization balance in Titan's nightside ionosphere, *Icarus*, *248*, 539–546, doi:10.1016/j.icarus.2014.11.012.
- Vuitton, V., P. Lavvas, R. V. Yelle, M. Galand, A. Wellbrock, G. R. Lewis, A. J. Coates, and J.-E. Wahlund (2009), Negative ion chemistry in Titan's upper atmosphere, *Planet. Space Sci.*, *57*(13), 1558–1572, doi:10.1016/j.pss.2009.04.004.
- Wahlund, J.-E. (2005), Cassini measurements of cold plasma in the ionosphere of Titan, *Science*, *308*(5724), 986–989, doi:10.1126/science.1109807.
- Wahlund, J.-E., et al. (2009), On the amount of heavy molecular ions in Titan's ionosphere, *Planet. Space Sci.*, *57*(14–15), 1857–1865, doi:10.1016/j.pss.2009.07.014.
- Waite, J. H., et al. (2004), The Cassini Ion and Neutral Mass Spectrometer (INMS) investigation, *Space Sci. Rev.*, *114*(1–4), 113–231, doi:10.1007/s11214-004-1408-2.
- Waite, J. H., D. T. Young, T. E. Cravens, A. J. Coates, F. J. Carry, B. Magee, and J. Westlake (2007), The process of tholin formation in Titan's upper atmosphere, *Science*, *316*(5826), 870–875, doi:10.1126/science.1139727.
- Waite, J. H., D. T. Young, J. H. Westlake, J. I. Lunine, C. P. McKay, and W. S. Lewis (2009), High-altitude production of Titan's aerosols, in *Titan from Cassini-Huygens*, edited by R. H. Brown, J.-P. Lebreton, and J. H. Waite, pp. 201–214, Springer Netherlands, Dordrecht.
- Wellbrock, A., A. J. Coates, G. H. Jones, G. R. Lewis, and J. H. Waite (2013), Cassini CAPS-ELS observations of negative ions in Titan's ionosphere: Trends of density with altitude, *Geophys. Res. Lett.*, *40*, 4481–4485, doi:10.1002/grl.50751.
- Whipple, E. C. (1965), The equilibrium electric potential of a body in the upper atmosphere and in interplanetary space, PhD thesis, The George Washington Univ., Washington, D. C.
- Whipple, E. C., T. G. Northrop, and D. A. Mendis (1985), The electrostatics of a dusty plasma, *J. Geophys. Res.*, *90*, 7405, doi:10.1029/JA090iA08p07405.
- Young, D. T., et al. (2004), Cassini Plasma Spectrometer Investigation, *Space Sci. Rev.*, *114*(1–4), 1–112, doi:10.1007/s11214-004-1406-4.